Interacting pairs of periodic solutions lead to tori in lasers subject to delayed feedback

D. Pieroux and T. Erneux
Université Libre de Bruxelles, Optique Nonlinéaire Théorique, Campus Plaine, C.P. 231, B-1050 Bruxelles, Belgium

T. Luzyanina* and K. Engelborghs
Katholieke Universiteit Leuven, Department of Computer Science, Celestijnenlaan 200A, B-3001 Heverlee, Belgium
(Received 29 August 2000; published 26 February 2001)

Models of class-B lasers subject to either an optoelectronic or an optical feedback are investigated analytically and numerically. We derive slow time amplitude equations from the laser delay differential equations and find multiple bifurcating and isolated branches of periodic solutions. We then show that secondary bifurcations to tori result from the interaction of pairs of Hopf bifurcations. The branches emerging from these bifurcations are followed numerically using a continuation method developed for delay differential equations.

DOI: 10.1103/PhysRevE.63.036211 PACS number(s): 42.65.Sf, 42.60.Mi, 05.45.−a

I. INTRODUCTION

Most class-B lasers [1], among which include CO_2, solid state and semiconductor (SC) lasers, are very sensitive to optical or optoelectronic delayed feedback. For instance, a tiny optical feedback such as the back-reflection of a SC laser beam into the laser cavity can lead to chaotic regimes [2]. The poor stability of these lasers is due to the fact that they are weakly damped nonlinear oscillators [3–6]. While feedback may lead to unwanted instabilities, a small feedback rate and a judicious choice of the delay may also produce desired high-frequency pulsating outputs [7–10].

Because lasers subject to a delayed feedback are nonlinear infinite-dimensional systems [11], they display a wide range of steady, oscillating, pulsating and chaotic regimes. Coexistence between those regimes is also very common. Some dynamical responses such as the low frequency fluctuations (LFF) [12,13] have only been observed for particular lasers but other bifurcation features are shared by different class-B laser systems [14,15].

Four types of feedback are commonly associated with lasers, namely, the coherent optical feedback, the incoherent optical feedback, the optoelectronic feedback acting on the pump and the optoelectronic feedback acting on the losses. The coherent optical feedback consists in the partial back-reflection of the light beam into the laser cavity. Because light propagates at a finite speed, it takes time for the beam to reenter the cavity. SC lasers are particularly sensitive to this type of feedback because they combine low facet reflectiveness and high gain. Moreover, dynamical frequencies of SC lasers are typically a few GHz. Therefore, a delay of a few hundreds of picoseconds, or equivalently an extra-cavity round-trip of a few centimeters, is enough for the delay to play a major role in the system dynamics. The simplest model describing a longitudinal single mode SC laser subject to a weak optical feedback has been formulated in 1980 by Lang and Kobayashi (LK) [16]. It consists in two nonlinear delay differential equations (DDEs) for the complex electrical field and the electronic carrier density. Numerical simulations of these equations successfully reproduce the dominant effects observed experimentally, such as mode-hopping, coexisting dynamical regimes and different forms of chaotic attractors such as LFF.

The simplest model of a laser controlled by an incoherent optical feedback was first proposed and studied by Otsuka and Chern [8] with the goal of designing high-frequency self-pulsating lasers. This model is a simplification of the feedback scheme proposed by Yasaka *et al.* [17] for stabilizing the laser frequency and reducing its linewidth. By contrast to the coherent optical feedback experiment, the laser beam passes through a polarization-rotation element that rotates the beam polarization by $\pi/2$ rad. As a result, the feedback field does not interact coherently with the intracavity field since their respective polarizations are orthogonal. The model of Otsuka and Chern [8] is formulated using two nonlinear DDEs, one for the laser intensity and the other for the population inversion (or the carrier density). Yen and coworkers [7] have successfully set up a SC laser system using this feedback to produce optical impulsions in the GHz range.

In the case of optoelectronic feedback, a photodetector converts the light intensity into an electrical signal that controls either the pump or the cavity losses [18,19]. The simplest models of these laser systems are described by two nonlinear DDEs for the laser intensity and the population inversion. A third equation taking into account the dynamics of the electronic feedback loop is sometimes added [18,20,21].

Whatever the feedback scheme, most of our knowledge on the dynamics of lasers controlled by delayed feedback comes from experiments or numerical simulations of the models. Indeed, except for the steady states, analytical results remain rare. This comes from the simultaneous presence of two mathematical difficulties: the laser intrinsic nonlinearity and the time lag involved in the feedback. To overcome these difficulties, different analytical methods have been proposed. Lasers exhibiting strongly pulsating intensities have been studied in [9,22,23] and approximations of the solution for specifically chosen time intervals have been determined. A second method consists in looking for

*On leave from the Institute of Mathematical Problems in Biology, Pushchino, Moscow region, Russia.

small amplitude periodic solutions. Using bifurcation techniques, it is then possible to derive amplitude equations describing the long time behavior of the laser [15,24]. We may also take advantage of the weak damping of the laser relaxation oscillations and reformulate the original laser equations as the equations for a weakly perturbed conservative oscillator [10,14,25]. Simple analytical expressions for the small amplitude nearly harmonic regimes as well as the large amplitude pulsating regimes can then be obtained. Giacomelli and coworkers proposed a fourth approach valid for large delays by formulating a partial differential equation from the DDEs [26].

In this paper, we use bifurcation techniques and derive slow time equations for the amplitude of the laser relaxation oscillations. Amplitude equations have been derived in the past for lasers subject to feedback but our analysis differs by the following points. First, we assume that the delay is sufficiently large so that it still appears in the slow time amplitude equation. We show that it is responsible for multiple bifurcating or isolated branches of periodic solutions. Second, we concentrate on the multiple branches of time-periodic intensities and propose a bifurcation mechanism for the appearance of quasiperiodic regimes. Specifically, we show analytically that this mechanism results from the interaction of two Hopf bifurcation points. It involves two periodic branches of opposite direction and is responsible for a secondary bifurcation to a T^2 torus followed by a tertiary bifurcation to a T^3 torus [27,28]. Moreover, the torus bifurcation persists even if one or both of the two Hopf bifurcation points have disappeared from the bifurcation diagram as a parameter is changed. The bifurcations to tori are important because they are quickly followed by more complex time-dependent outputs as the control parameter is further changed. This motivates our combined analytical and numerical study of these bifurcations. Third, we investigate the validity of our asymptotic results by comparing diagrams obtained from the amplitude equation and from the original laser equations. To this end, we use a continuation method which has recently been developed for DDEs [29]. It is the first application of a continuation method for a laser problem formulated in terms of delay differential equations.

The plan of the paper is as follows. In Sec. II, we briefly review a series of laser problems and derive a common slow time amplitude equation. In Sec. III, we investigate the bifurcation diagram of a laser subject to a weak optoelectronic feedback acting on the pump. Steady, periodic and quasiperiodic solutions are found and their stability properties are investigated. In Sec. IV, we compare the bifurcation diagrams obtained from the laser original equations and from the amplitude equations. Finally, we summarize in Sec. V the main points of our combined analytical and numerical study of lasers subject to delayed feedback.

II. THE REDUCED MODELS

In this section, we consider the four feedback schemes described in the introduction and derive a common slow time amplitude equation for the intensity of the laser field. We carried out the analysis with the symbolic manipulator MATHEMATICA and we chose the coefficients in the perturbation expansions so that the final result is similar for each feedback scheme.

A. Optoelectronic and incoherent optical feedback

The behavior of the intensity I and excess carrier number N of a longitudinally single mode SC laser subject to either an optoelectronic or an incoherent optical delayed feedback is described by the following set of DDEs [8,9,20]:

$$\frac{dI}{dt}=\left(\frac{N}{1+g_{sat}I}-1-\alpha\overline{I}\right)I+e_{sp}(N+N_a), \tag{1a}$$

$$T\frac{dN}{dt}=P-N-\frac{N(I+\beta\overline{I})}{1+g_{sat}I}+\gamma\overline{I} \tag{1b}$$

where the delay τ appears in $\overline{I}\equiv I(t-\tau)$. In these equations, time t is measured in units of the photon lifetime τ_p, $T=\tau_s/\tau_p$ with τ_s the carrier lifetime, P is the pumping rate above threshold, e_{sp} is the spontaneous emission rate, N_a is the excess carrier number at transparency and g_{sat} is the gain saturation coefficient [30]. The coefficients α, β and γ are proportional to the feedback rate [15]. For an optoelectronic feedback acting on the laser losses, $\alpha\neq 0$ and $\beta=\gamma=0$. For an optoelectronic feedback acting on the pump, $\gamma\neq 0$ and $\alpha=\beta=0$. For an incoherent optical feedback, $\beta\neq 0$ and $\alpha=\gamma=0$. Equations (1a) and (1b) also hold for two-level class-B lasers with N being the population inversion and $g_{\mathrm{sat}}\equiv 0$.

In the absence of feedback, Eqs. (1a) and (1b) admit a single stable steady state $(I,N)=(I_0,N_0)$. It is given in parametric form as

$$P=N_0\left(1+\frac{I_0}{1+g_{sat}I_0}\right), \tag{2a}$$

$$N_0=\frac{(1+g_{sat}I_0)(I_0-e_{sp}N_a)}{I_0+e_{sp}(1+g_{sat}I_0)}, \tag{2b}$$

where $I_0>0$ is the parameter. If the feedback is sufficiently small, the laser operates in the vicinity of (I_0,N_0). In order to study small amplitude oscillating solutions, it is mathematically convenient to rescale time with respect to the laser relaxation oscillation frequency $\omega_r=\sqrt{I_0/T}$ and to introduce the deviations of I and N from $I=I_0$ and $N=N_0$. Specifically, we introduce the time s and the variables y and n defined by

$$s=\omega_r t, \tag{3a}$$

$$I=I_0(1+\sqrt{6}\,y),\quad N=N_0+\sqrt{6}\,\omega_r n. \tag{3b}$$

The coefficients of y and n in Eq. (3b) are chosen such that the large T parameter that ranges from 10^3 for SC lasers up to 5×10^5 for solid-state lasers can be removed from Eq. (1b). The feedback rates α, β and γ as well as the spontaneous emission rate e_{sp} and the gain saturation term g_{sat} are

typically small. This suggest to simplify Eqs. (1a) and (1b) by properly scaling all parameters. We first introduce a small parameter $\epsilon \ll 1$ defined by

$$\epsilon = \left[\frac{(1+I_0)^2}{4I_0} \frac{1}{T} \right]^{1/4} \tag{4}$$

and then expand the parameters α, β, γ, e_{sp} and g_{sat} as

$$\alpha = \frac{4}{1+I_0} \epsilon^4 C_\alpha + \cdots, \tag{5a}$$

$$\beta = 2\epsilon^2 C_\beta + \cdots, \tag{5b}$$

$$\gamma = 2\epsilon^2 C_\gamma + \cdots, \tag{5c}$$

$$g_{sat} = \frac{4}{1+I_0} \epsilon^4 g + \cdots, \tag{5d}$$

$$e_{sp} = \frac{4I_0^2}{(1+N_a)(1+I_0)} \epsilon^4 e + \cdots. \tag{5e}$$

In Eqs. (4) and (5), coefficients depending on I_0 are introduced in order to simplify our final amplitude equation. In what follows, we consider one of the feedback rates as our control parameter. Consequently, I_0 is always constant and the limit ϵ small means the limit T large. The new parameters g, e, C_α, C_β, and C_γ are treated as $O(1)$ quantities in this limit. After introducing Eqs. (3)–(5) into Eqs. (1a) and (1b), we seek a two-time solution of the form

$$y = \epsilon y_1(s,\sigma) + \epsilon^2 y_2(s,\sigma) + \cdots, \tag{6a}$$

$$n = \epsilon n_1(s,\sigma) + \epsilon^2 n_2(s,\sigma) + \cdots, \tag{6b}$$

where σ is a new slow time variable defined by

$$\sigma = \epsilon^2 s. \tag{7}$$

We note that $\overline{y} = y(s-\theta) \equiv y(s-\theta, \sigma - \Theta)$ with the rescaled delays θ and Θ defined by

$$\theta = \omega_r \tau \quad \text{and} \quad \Theta = \epsilon^2 \theta. \tag{8}$$

Furthermore, s and σ are treated as independent variables and this implies the chain rule $d/ds = \partial/\partial s + \epsilon^2 \partial/\partial\sigma$. Introducing Eqs. (6a) and (6b) into the equations for y and n and equating to zero the coefficients of each power of ϵ lead to a sequence of linear problems for the unknowns functions (y_i, n_i), $i = 1,2,\ldots$. We solve each problem sequentially. The analysis requires to solve the first two problems and then to apply a solvability condition to the $O(\epsilon^3)$ problem. The procedure is tedious but straightforward and we omit all details. The leading solution is given by

$$y(s,\sigma) = \epsilon(A(\sigma)e^{is} + \text{c.c.}) + O(\epsilon^2), \tag{9a}$$

$$n(s,\sigma) = \epsilon(A(\sigma) i e^{is} + \text{c.c.}) + O(\epsilon^2), \tag{9b}$$

where c.c. means complex conjugate. The evolution of the slow time amplitude A is determined by the following equation:

$$\frac{dA}{d\sigma} = -(1 + e + g + iC_\beta - iC_\gamma)A - i|A|^2 A - (C_\alpha - iC_\beta + iC_\gamma) e^{-i\theta} \overline{A}, \tag{10}$$

with $\overline{A} \equiv A(\sigma - \Theta)$. We discuss the solutions of this equation in the next section.

B. Coherent optical feedback

The LK model for a longitudinally single mode SC laser controlled by a weak optical feedback is [16]

$$\frac{d\mathcal{E}}{dt} = \frac{1+i\alpha}{2} \left(\frac{N}{1 + g_{sat}|\mathcal{E}|^2} - 1 \right) \mathcal{E} + \eta e^{-i\Omega\tau} \overline{\mathcal{E}}, \tag{11a}$$

$$T\frac{dN}{dt} = P - N - \frac{N|\mathcal{E}|^2}{1 + g_{sat}|\mathcal{E}|^2}, \tag{11b}$$

with $\mathcal{E}$ the complex electromagnetic field, $\overline{\mathcal{E}} \equiv \mathcal{E}(t-\tau)$, α the linewidth enhancement factor, η the normalized feedback rate and Ω the dimensionless optical frequency of the laser without feedback. The other variables and parameters are defined in the previous section. Equations (11a) and (11b) also model two-level class-B lasers subject to optical feedback if g_{sat} and α are set to zero. As previously, we investigate the response of the laser to a weak feedback. Our analysis of Eqs. (11a) and (11b) is similar to that of Eqs. (1a) and (1b). We write the field as $\mathcal{E}(t) = \mathcal{R}(t) e^{i\phi(t)}$ and introduce the deviations of $\mathcal{R}$ and N relative to the $\eta = 0$ steady state. Specifically, we introduce the new variables r and n defined by

$$\mathcal{R} = \mathcal{R}_0 \left(1 + \sqrt{\frac{3}{2}} r \right), \quad N = N_0 + \sqrt{\frac{6I_0}{T}} n \tag{12}$$

with $\mathcal{R}_0 = \sqrt{I_0}$, $I_0 = (P-1)/(1+g_{\text{sat}})$ and $N_0 = 1 + g_{sat} I_0$. We also introduce the slow time s defined by Eq. (3a) and we expand η as

$$\eta = \frac{4I_0}{1+I_0} \epsilon^4 C_\eta + \cdots, \tag{13}$$

with $C_\eta = O(1)$ and ϵ defined by Eq. (4). We then seek a solution of the form

$$r = \epsilon r_1(s,\sigma) + \epsilon^2 r_2(s,\sigma) + \cdots, \tag{14a}$$

$$n = \epsilon n_1(s,\sigma) + \epsilon^2 n_2(s,\sigma) + \cdots, \tag{14b}$$

$$\phi = \phi_0(s,\sigma) + \sqrt{3/2}(\epsilon\phi_1(s,\sigma) + \epsilon^2 \phi_2(s,\sigma) + \cdots). \tag{14c}$$

Introducing Eqs. (14a)-(14c) into the equations for r, n and ϕ lead to a sequence of problems for the functions r_1,

TABLE I. Values of the parameters ξ_r, ξ_i, and ψ appearing in Eq. (19).

Feedback scheme	ξ_r	ξ_i	ψ
Optoelectronic (losses)	0	0	π
Optoelectronic (pump)	0	-1	$-\pi/2$
Incoherent optical	0	$+1$	$\pi/2$
Coherent optical	$+1$	0	0

$r_2, \ldots$ which we solve sequentially. The first two problems for ϕ imply that ϕ_0 depends only on the slow time σ and satisfies

$$\frac{d\phi_0}{d\sigma} = -\tilde{C}\sin(\tau\Omega + \arctan(\alpha) + \phi_0 - \overline{\phi_0}), \tag{15}$$

where $\tilde{C} = 2\sqrt{1+\alpha^2}C_\eta$, $\overline{\phi_0} = \phi_0(\sigma - \Theta)$ and Θ is defined by Eq. (8). Note that this phase equation can be obtained directly from the LK equations by neglecting the intensity variation [31]. Equation (15) admits a solution of the form $\phi_0 = \omega\sigma$ where ω is the optical frequency shift caused by the feedback. Substituting $\phi_0 = \omega\sigma$ into Eq. (15) leads to a transcendental equation for ω:

$$\omega + \tilde{C}\sin(\tau\Omega + \arctan(\alpha) + \Theta\omega) = 0. \tag{16}$$

The roots of Eq. (16) correspond to the so-called modes and anti-modes of the external cavity. A linear stability analysis shows that solutions are stable if $\tilde{C}\Theta\cos(\tau\Omega + \arctan(\alpha) + \Theta\omega) + 1 > 0$. Assuming that ϕ_0 has reached a stable steady state, the solution for r and n is time-periodic and is given by

$$r(s,\sigma) = \epsilon(A(\sigma)e^{is} + \text{c.c.}) + O(\epsilon^2), \tag{17a}$$

$$n(s,\sigma) = \epsilon(A(\sigma)ie^{is} + \text{c.c.}) + O(\epsilon^2), \tag{17b}$$

where A, the complex envelope of the oscillations, satisfies

$$\frac{dA}{d\sigma} = -(1+g+\hat{C})A - i|A|^2A + \hat{C}e^{-i\theta}\overline{A}, \tag{18}$$

with $\hat{C} = \sqrt{1+\alpha^2}\cos(\tau\Omega - \arctan(\alpha) + \Theta\omega)C_\eta$. We have verified that Eq. (18) linearized around $A=0$ admits a periodic solution $A = \exp(i\mu\sigma)$ and that the conditions for μ and $\hat{C}$ match the Hopf bifurcation conditions derived by Ritter and Haug [32] (see review in [33]) in the absence of gain saturation.

In summary, Eqs. (10) and (18) are particular cases of the more general equation

$$\frac{dA}{d\sigma} = -(1+e+g+(\xi_r + i\xi_i)C)A - i|A|^2A + Ce^{-i(\theta-\psi)}\overline{A}, \tag{19}$$

with $\overline{A} = A(\sigma - \Theta)$ and $\Theta = \epsilon^2\theta$. The parameters ξ_r, ξ_i, and ψ are documented in Table I for the four feedback schemes. It is instructive to review the significance of each term in the right hand side of Eq. (19). The term $-(1+e+g)A$ accounts for the linear damping of the laser oscillation in the absence of feedback. The nonlinear term $i|A|^2A$ is the first order nonlinear correction to the laser frequency. The term $-(\xi_r + i\xi_i)CA$ takes into account the change of the damping rate and the shift of the laser optical frequency caused by the feedback. Finally, the term $Ce^{-i(\theta-\psi)}\overline{A}$ is the delayed contribution of the feedback.

If $\theta = O(1)$, then $\Theta = \epsilon^2\theta$ is a small quantity and this implies $\overline{A} \simeq A$. As a result, Eq. (19) simplifies to an ordinary differential equation (ODE) at first order. Similar normal-form ODEs have been proposed previously for lasers subjected to moderate incoherent optical feedback [24] or to moderate optoelectronic feedback [15]. However, if θ is $O(\epsilon^{-2})$ large, we need to investigate the DDE (19) [15,34].

III. STEADY, PERIODIC, AND QUASIPERIODIC REGIMES

In this section, we analyze the bifurcation diagram of a class-B laser controlled by a weak optoelectronic feedback acting on the pump. We set $C_\alpha = C_\beta = 0$ and $C_\gamma = C$ in Eq. (10) and, by rescaling A, σ, and C, we eliminate the parameters e and g. Equation (10) then becomes

$$\frac{dA}{d\sigma} = -(1-iC)A - i|A|^2A - iCe^{-i\theta}\overline{A}. \tag{20}$$

The results presented here extend those found in [34]. Note that, as discussed in the previous section, similar results are expected for the other feedback schemes.

A. Steady and periodic states

The trivial solution $A=0$ corresponds to the laser steady state $(I,N) = (I_0, N_0)$ and solutions of the form $A = R\exp(i\nu\sigma)$ with R and ν constant correspond to periodic regimes of the laser. Substituting $A = R\exp(i\nu\sigma)$ into Eq. (20), using Eq. (8) and separating the real and imaginary parts lead to two following equations for R and ν:

$$1 + C\sin((1+\epsilon^2\nu)) = 0, \tag{21a}$$

$$R^2 + \nu + \tan\left(\frac{(1+\epsilon^2\nu)\theta}{2}\right) = 0. \tag{21b}$$

As demonstrated by Eq. (21a), periodic regimes exist only for $|C| \geqslant 1$. The multiple solutions of Eqs. (21a) and (21b) are best analyzed by changing ν continuously from $-\infty$ to ∞. As shown in Fig. 1, there are several branches of periodic solutions. We first consider the branches that emerge from the zero solution at Hopf bifurcation points. These are found by setting $R=0$ in Eq. (21b). We then obtain an equation for the Hopf bifurcation frequencies $\nu = \nu_H$ given by

$$0 = \nu_H + \tan\left(\frac{(1+\epsilon^2\nu_H)\theta}{2}\right). \tag{22}$$

As illustrated in Fig. 2, Eq. (22) admits an infinite number of solutions ν_H for each fixed value of the delay θ. Knowing

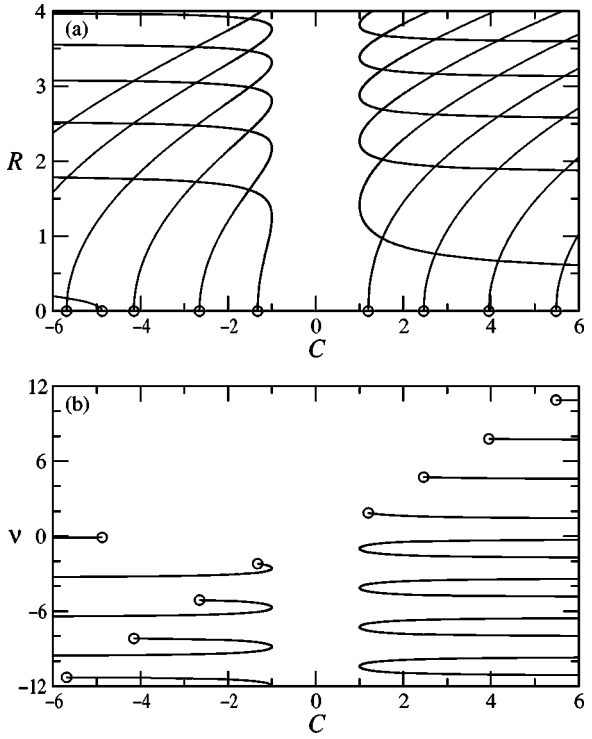

FIG. 1. Periodic regimes obtained from the reduced model Eq. (20). We represent (a) the amplitude R and (b) the frequency ν as functions of C. The trivial solution $R=0$ corresponds to the laser steady state and the constant $R\neq 0$ solutions correspond to time-periodic regimes. Circles mark Hopf bifurcations. Fixed parameters: $\theta\simeq 63.25$ and $\Theta=2$. They are determined using Eqs. (4) and (8) with $I_0=1$, $T=1000$ and $\tau=2000$.

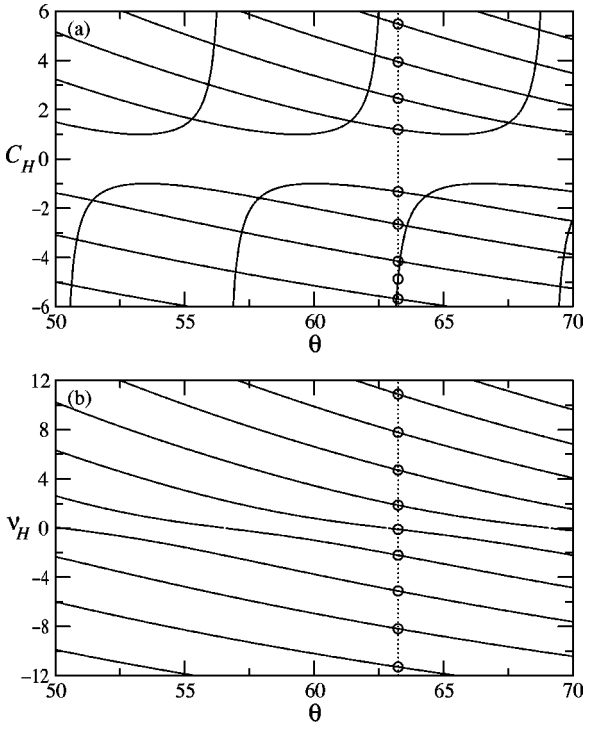

FIG. 2. Hopf bifurcation curves obtained from the reduced model Eq. (20). We represent (a) C_H and (b) ν_H as functions of the delay θ. They are obtained from Eqs. (22) and (23) using Eq. (4) with $I_0=1$ and $T=1000$. The circles mark the Hopf bifurcation points shown in Fig. 1.

ν_H, we determine the feedback rate $C=C_H$ from Eq. (21a). Using trigonometric identities, it comes

$$C_H=\frac{1+\nu_H^2}{2\nu_H}. \tag{23}$$

The direction of bifurcation is determined by analyzing Eqs. (21a) and (21b) in the neighborhood of the Hopf bifurcation point. We find that the Hopf bifurcation is supercritical or subcritical if $\cos((1+\epsilon^2\nu_H)\theta)<0$ or $\cos((1+\epsilon^2\nu_H)\theta)>0$, respectively. If $\cos((1+\epsilon^2\nu_H)\theta)=0$, or equivalently if

$$(1+\epsilon^2\nu_H)\theta=\pm\frac{\pi}{2}+m2\pi, \tag{24}$$

the Hopf bifurcation is vertical, in first approximation. From Eqs. (21a) and (22), we then find $C_H=\mp 1$ and $\nu_H=\mp 1$. Finally, substituting $\nu_H=\mp 1$ into Eq. (24) gives

$$\theta=\theta_m^*=\frac{\pm\frac{\pi}{2}+m2\pi}{1\mp\epsilon^2}. \tag{25}$$

By analyzing the direction of bifurcation in the neighborhood of θ_m^*, we conclude that the m^{th} Hopf bifurcation is supercritical for $\theta<\theta_m^*$ and subcritical for $\theta>\theta_m^*$.

Figure 1 shows that there also exist isolated branches of periodic solutions. For clarity, we shall restrain our discussion to the branches located in the $C_H>0$ half plane, but similar arguments hold for the other branches. The existence of isolated branches can be explained simply by considering a Hopf bifurcation line in Fig. 2 and by following its behavior as the delay θ is increased continuously from zero. We note that the m^{th} Hopf bifurcation point exhibits a decreasing C_H and is supercritical for $\theta<\theta_m^*$ [Fig. 3(a)]. At $\theta=\theta_m^*$, $C_H=1$ and the bifurcation is vertical. For $\theta>\theta_m^*$, the bifurcation is subcritical [Figs. 3(b) and 3(c)] and C_H quickly increases. The emerging branch folds back at a limit point located at $C=1$. Finally, $C_H\to\infty$ as $\theta\to\theta_m^\infty$ where θ_m^∞ is the limit of θ as $C\to\infty$. Using Eqs. (21a) and (22), we find that $\nu_H^\infty=0$ and $\theta_m^\infty=m2\pi$. If $\theta>\theta_m^\infty$, the Hopf bifurcation point has disappeared but the periodic solution remains in the form of two branches connected by the limit point of the previously bifurcating branch [Fig. 3(d)].

B. Stability analysis

In [34], we investigated the stability of the steady and periodic solutions of Eq. (20). We found that the steady state $A=0$ is stable for sufficiently low values of $|C|$. Increasing $|C|$ progressively from zero, a Hopf bifurcation leads to a stable (unstable) periodic solution if the bifurcation is supercritical (subcritical). All branches emerging from the other primary Hopf bifurcations for larger value of $|C|$ are unstable. Both subcritical and isolated branches of periodic so-

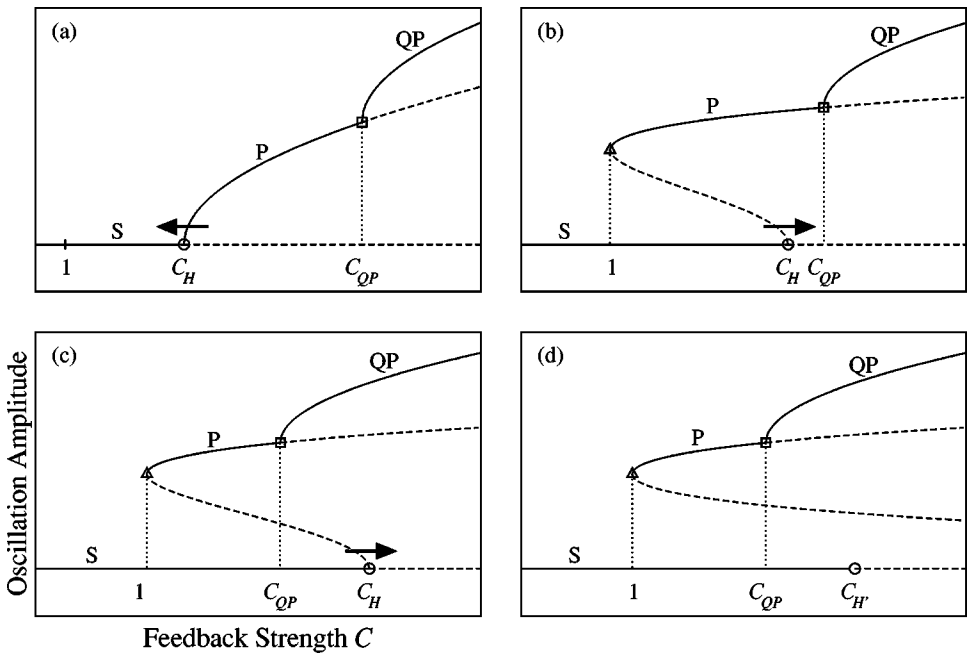

FIG. 3. Qualitative bifurcation diagrams deduced from the reduced model Eq. (20). Case $C>0$. The maximum of the oscillations is represented as a function of C. C_H and $C_{H'}$ (C_{QP}) denote Hopf (torus) bifurcation points. Labels S, P, and QP design branches of steady, periodic and quasiperiodic regimes, respectively. Full (dotted) lines represent stable (unstable) regimes. Circles mark Hopf bifurcation points, squares denote torus bifurcation points and triangles correspond to limit points. The sequence of figures (a) to (d) shows how a periodic branch evolves as θ is gradually increased. The arrows indicate that C_H decreases if the bifurcation is supercritical (a) and increases if it is subcritical [(b) and (c)]. As $\theta\rightarrow\theta_m^{\infty}$, the point C_H moves to infinity and the branch becomes isolated for $\theta>\theta_m^{\infty}$ (d). For clarity reason, only one branch is displayed.

lutions experience a turning point (limit point) at $|C|=1$. Close to their respective limit point, the upper and lower branches of solutions are stable and unstable, respectively. Torus bifurcations to quasiperiodic oscillations are found on every branch of periodic solutions.

In Fig. 4, Hopf (full lines) and torus (dashed lines) bifurcation curves are shown for a limited range of values of C

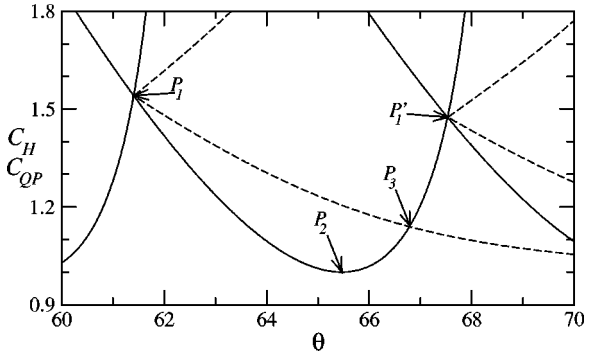

FIG. 4. Hopf and first torus bifurcation curves obtained from the reduced model Eq. (20). We represent C_H and C_{QP} as functions of θ by solid and broken lines, respectively. At P_1 and P_1', two Hopf bifurcation points collide and a torus bifurcation appears on each of the two branches of periodic solutions. At P_2, the Hopf bifurcation is vertical and switches from supercriticality for $\theta<\theta_{P_2}$ to subcritical for $\theta>\theta_{P_2}$. At P_3, the Hopf and first torus bifurcation points of the same bifurcating branch coexist for a different amplitude R. Fixed parameters: same as in Fig. 2.

and θ. For simplicity, we consider here the case $C_H>0$ but similar results have been found for $C_H<0$. Four particular points are identified. Point P_1 corresponds to the collision of two Hopf bifurcation points exhibiting two distinct frequencies. A secondary torus bifurcation is also created on each of the two bifurcating branches. At point P_2, $C_H=1$ and the periodic branch is vertical, as seen in the previous section. At point P_3, the Hopf and first torus bifurcation points of the bifurcating branch coexist at the same value of C but for a different amplitude R. Finally, point P_1' is equivalent to point P_1, i.e., it corresponds to another collision of two Hopf bifurcation points. By increasing further θ beyond P_1', there is a point P_2' for which $C_H=1$, then a point P_3' displaying the same properties as P_3. By increasing the delay, this sequence of three points repeats endlessly.

Depending on the value of θ, three different cases are possible for the destabilization of the steady state. If $\theta_{P_1}<\theta<\theta_{P_2}$, a branch of stable periodic solutions emerges from the Hopf bifurcation point at $C=C_H$ [Fig. 3(a)]. This branch of solutions admits a secondary torus bifurcation at $C=C_{QP}$ which leads to quasiperiodic oscillations. If $\theta_{P_2}<\theta<\theta_{P_3}$, the Hopf bifurcation at $C=C_H$ is subcritical and leads to unstable periodic solutions [Fig. 3(b)]. As seen before, the branch folds back at the limit point located at $C=1$. The periodic solutions are stable right after the turning point. There is thus bistability between steady and periodic regimes leading to a hysteresis behavior. As in the previous case, a secondary torus bifurcation is found at $C=C_{QP}$

$>C_H$. If $\theta_{P_3}<\theta<\theta_{P_1'}$, then $C_{QP}<C_H$ [Fig. 3(c)] and bistability between steady and periodic regimes on the one hand, and steady and quasiperiodic regimes on the other hand leads to hysteresis between these three regimes. For instance, consider a laser in its steady state for $C<C_H$ and start increasing C. Once C surpasses C_H, the regime switches from steadiness to quasiperiodicity. Decreasing then C, the regime stays quasiperiodic until C becomes smaller than C_{QP}. For $1 \leqslant C \leqslant C_{QP}$, the regime is periodic. As C is decreased below 1, the laser state jumps back from the periodic branch to the steady one. As explained previously, Fig. 3(d) shows that the branch becomes isolated for θ larger than its corresponding θ_m^{∞}.

C. Collision of two Hopf bifurcations

Points P_1 and P_1' of Fig. 4 are examples of double Hopf bifurcation points. Here two Hopf bifurcations collide and two secondary torus bifurcations appear. This is possible because Eq. (20) linearized around $|A|=0$ admits two eigenpairs on the imaginary axis. We investigate this phenomenon by analyzing the solution of Eq. (20) in the neighborhood of point P_1. A particular feature of our bifurcation problem is that the branches emerging from the two Hopf bifurcation points have opposite direction of bifurcation as they collide. All mathematical details are given in the appendix and the main results are summarized in Fig. 5. In this figure, the amplitude of the solution is represented as a function of the deviation $C_2 \propto C - C_{P_1}$ defined by Eq. (A2).

If θ is slightly smaller than θ_{P_1}, the steady state is destabilized by a subcritical bifurcation. There is no torus bifurcation point and both primary Hopf branches [P_1 and P_2 in Fig. 5(a)] are unstable. On the other hand, if θ is slightly greater than θ_{P_1}, the first Hopf bifurcation is supercritical and leads to a branch of stable periodic solutions [branch P_1 in Fig. 5(b)]. Increasing C further, the branch P_1 undergoes a supercritical torus bifurcation from which a branch of stable two-frequency quasiperiodic oscillations emerges [QP in Fig. 5(b)]. This quasiperiodic branch is itself destabilized by a tertiary bifurcation to a three-frequency quasiperiodic regime. At the bifurcation point, we have verified that $\min_{\sigma}(|A(\sigma)|)=0$. Increasing C further, the unstable part of the QP branch disappears at a torus bifurcation point located on the branch P_2. Note that, at first order, the amplitude of the closed QP branch is proportional to the square root of the distance between the two Hopf bifurcation points, as shown by the scaling used in Eqs. (A1), (A2), and (A5).

In summary, we have demonstrated that torus bifurcations naturally result from interacting pairs of Hopf bifurcations. As explained before, branches emerging from the steady state $|A|=0$ become isolated as their Hopf bifurcation point moves to infinity for increasing θ. Because the isolated branches possess no more Hopf bifurcation points, they experience no new torus bifurcation creation. However, existing bifurcations remain.

IV. NUMERICAL RESULTS

In the previous sections, we used asymptotic methods to construct small amplitude solutions of the laser equations. In this section, we investigate these equations numerically in order to check and extend the domain of validity of our analytical results. We consider again an optoelectronic feedback acting on the pump of the laser.

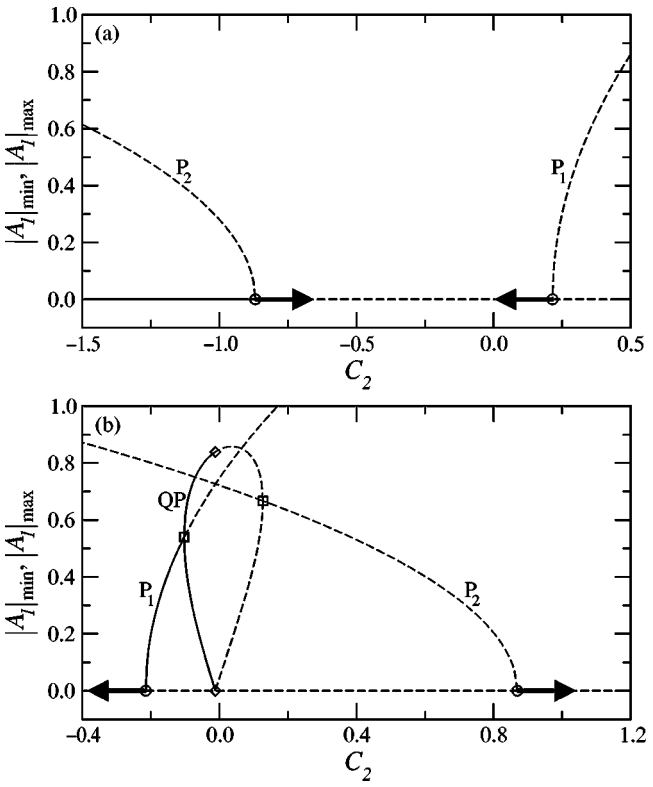

FIG. 5. Analytical bifurcation diagram of the reduced model Eq. (20) near the double Hopf point P_1 of Fig. 4. The laser steady state corresponds to the $|A|=0$ solution. Branches P_1 and P_2 of periodic regimes correspond to solutions for which $|A|\neq 0$ is constant. The branch QP of quasiperiodic regimes correspond to periodic solutions of $|A|$. Both the minima and maxima of $|A|$ are represented. We illustrate (a) the case $\theta<\theta_{P_1}$ and (b) the case $\theta>\theta_{P_1}$. The secondary torus bifurcations appear only if $\theta>\theta_{P_1}$. Full (dotted) lines represent stable (unstable) regimes. Circles and squares mark bifurcation points as in Fig. 3. The diamond marks a tertiary bifurcation point to T^3 tori. Fixed parameters: same as in Table II.

We integrated the full model Eqs. (1a) and (1b) and the reduced model Eq. (20) with a variable step size Runge-Kutta 4(3) method and Hermite interpolation [35]. We also used DDE-BIFTOOL, a Matlab continuation package which has recently been developed [29] and that allows the continuation of branches of stable and unstable steady and periodic solutions of DDEs. This is the first time that continuation methods are used for solving a laser problem which includes a delayed feedback. We used this package for the full and reduced models.

Figure 6(a) displays the numerical bifurcation diagram of Eqs. (1a) and (1b) with $\alpha=\beta=0$. The nonlinear gain saturation and the noise terms are neglected. As the feedback strength increases, we note that a stable periodic solution emerges from the steady state. This periodic regime then undergoes a secondary bifurcation to quasiperiodic oscillations. The quasiperiodic regime becomes unstable at a higher

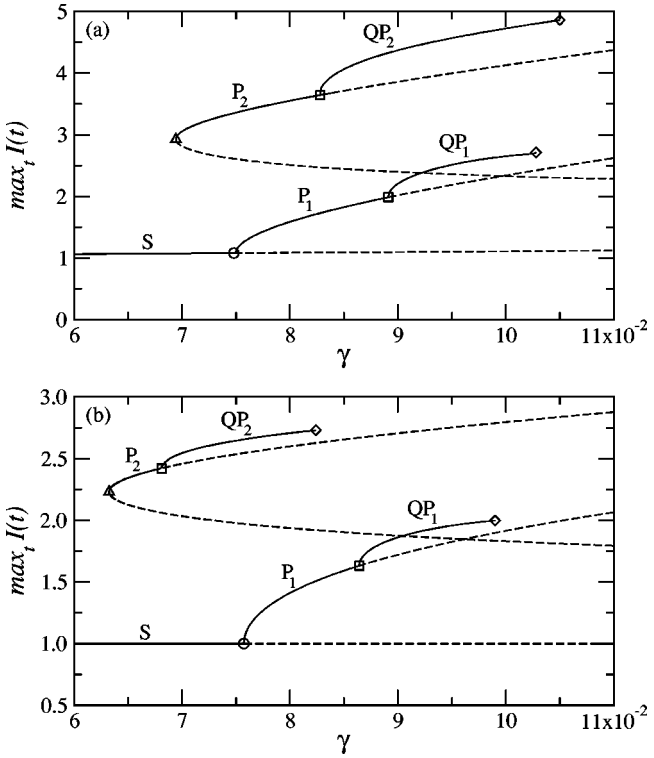

FIG. 6. Numerical bifurcation diagrams obtained from (a) the full model Eqs. (1a) and (1b) and (b) the reduced model Eq. (20). The maximal value of the intensity I is shown versus the feedback rate γ. The branches of unstable periodic solutions were computed with (a) the numerical continuation method and (b) by using Eqs. (21a) and (21b). The branches of stable quasiperiodic solutions were obtained by direct numerical integration of the equations. Steady, periodic, and quasiperiodic regimes are labeled S, P, and QP, respectively. Full (dotted) lines represent stable (unstable) regimes. Fixed parameters: $I_0=1$, $T=1000$, $\tau=2000$ and $\alpha=\beta=g_{sat}=e_{sp}=0$. Point marks: same as in Figs. 3 and 5.

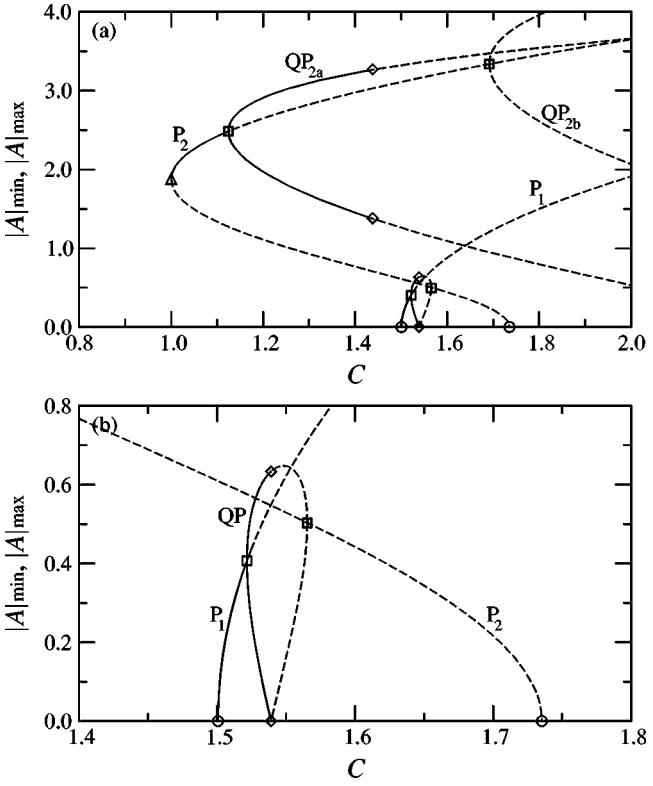

FIG. 7. Numerical bifurcation diagrams of Eq. (20) in the vicinity of the double Hopf bifurcation point P_1 of Fig. 4. These diagrams were obtained by using the numerical continuation method. Figure (b) is a blow up figure of part of Fig. (a). The meaning of the different curves, labels and marks is the same as in Figs. 3 and 5. Fixed parameters: $\theta=61.6$ and $\Theta\simeq 1.948$ corresponding to $I_0=1$, $T=1000$, and $\tau\simeq 1947.96$.

value of the feedback strength and the laser jumps towards another quasiperiodic regime which emerges from an isolated branch of periodic regimes. Increasing the feedback strength further leads to the destabilization of this quasiperiodic regime and to the appearance of chaos (not shown in the figure). However, if the feedback strength is reduced, the system state follows the isolated branch, exhibits periodic intensity oscillations for sufficiently low values of the feedback strength and finally jumps back to the steady state. The system exhibits thus bistability between bifurcating and isolated branches of solutions.

The bifurcation diagram of the reduced model Eq. (20) for the same values of the parameters is shown in Fig. 6(b). The quantitative agreement between the two diagrams is good for the branch emerging from the Hopf bifurcation point. The discrepancies are more important for the isolated branch. This is not surprising since Eq. (20) describes small amplitude solutions. Moreover, we chose $T=1000$ and $I_0=1$ for our simulations. These are typical values for SC lasers and lead to $\epsilon\simeq 0.18$. Solid-state lasers exhibit larger values of T implying a smaller ϵ. A better agreement for the isolated branch can then reasonably be expected. Nevertheless, we note from Fig. 6 that all the bifurcation features of the full laser equations are correctly captured by the reduced model.

Finally, we show in Fig. 7 the bifurcation diagram obtained directly from Eq. (20) for θ slightly larger than θ_{P_1}. In agreement with our asymptotic analysis (see Fig. 5), the first bifurcation is a supercritical Hopf bifurcation leading to the branch P_1 of periodic solutions. The periodic solutions then undergo a torus bifurcation giving rise to the branch QP of quasiperiodic oscillations. The other side of the QP emerges from the branch P_2 of unstable periodic solutions. Note that branch P_2 emerges subcritically, recovers its stability after it folds back and remains stable between its limit point and a second torus bifurcation point.

V. SUMMARY

In this work, we combined analytical and numerical techniques in order to investigate the bifurcation diagram of class-B lasers subject to a delayed feedback. The application of a numerical continuation method recently developed for DDEs played a key role in determining unstable branches of periodic and quasiperiodic solutions.

In the first part of this paper, we briefly reviewed a series of laser systems subject to a delayed feedback. Although each laser system is modeled by different equations, we ob-

tained similar amplitude equations for the laser relaxation oscillations. This observation had already been made before for lasers controlled by optoelectronic feedback [15] but is now also verified for lasers subject to coherent optical feedback. The advantages of studying slow time amplitude equations are threefold. First, we may determine useful analytical expressions for the periodic solutions and their stability boundaries in terms of the laser parameters. Second, we may use a continuation method and follow branches of stable and unstable quasiperiodic regimes since these correspond to branches of periodic solutions for the reduced equations. Note that, in practice, unstable quasiperiodic solutions are impossible to find by standard numerical methods alone. Third, the stiffness of the original equations has been removed, leading to a more efficient numerical processing.

In the second and main part of the paper, we investigated the bifurcation diagram of a specific laser problem. The branches of periodic and quasiperiodic solutions were studied analytically and numerically. We showed that the bifurcations to tori result from the interaction of two nearby Hopf bifurcations with two distinct frequencies. The quasiperiodic oscillations typically exhibit these frequencies. A tertiary bifurcation point from the T^2 torus to a T^3 torus was also demonstrated.

ACKNOWLEDGMENTS

This research has been supported by the US Air Force Office of Scientific Research Grant No. AFOSR F49620-95-0065, the National Science Foundation Grant No. DMS-9625843, Research Council K.U.Leuven (project OT/98/16), FNRS and FWO (Belgium), and the program on Interuniversity Poles of Attraction for Science, Technology and Culture (IUAP P4/02 and IUAP P4/07).

APPENDIX A: BIFURCATIONS NEAR DOUBLE HOPF POINTS

In this appendix, we study the solution of Eq. (20) in the vicinity of a double Hopf bifurcation point $(C,\theta)=(C_*,\theta_*)$. Points P_1 and P_1' of Fig. 4 are examples of such degenerate points. Because the analysis is tedious but straightforward, we used MATHEMATICA. At the double Hopf point, Eq. (20) linearized around (C_*,θ_*) admits two periodic solutions exhibiting two distinct frequencies. In order to determine the amplitude equations of these two periodic modes, we introduce a small parameter $\delta \ll 1$ defined by

$$\theta=\theta_*+\delta^2\theta_2, \tag{A1}$$

with $\theta_2=\pm 1$ and we expand the bifurcation parameter as

$$C=C_*+\delta^2 C_2+\cdots. \tag{A2}$$

We then seek a solution of Eq. (20) of the form

$$A=\delta A_1(\sigma,\rho)+\delta^2 A_2(\sigma,\rho)+\cdots, \tag{A3}$$

where ρ is a new slow time variable defined by

$$\rho\equiv\delta^2\sigma. \tag{A4}$$

Introducing expressions (A1)–(A3) into Eq. (20) and using the chain rule $d/d\sigma=\partial/\partial\sigma+\delta^2\partial/\partial\rho$ lead to a sequence of problems for the unknowns functions A_i, $i=1,2,\ldots$. This cascade of problems is solved sequentially. In first approximation, the solution is a linear combination of two periodic functions:

$$A=\delta(\hat{f}(\rho)e^{iF\sigma}+\hat{g}(\rho)e^{iG\sigma})+\mathcal{O}(\delta^2). \tag{A5}$$

The frequency F and G are the two distinct roots of Eq. (22) with $C_H=C_*$. The slow time evolution equation for $\hat{f}$ is

$$\frac{d\hat{f}}{d\rho}=\hat{f}\frac{(1+iF)C_2-C_*[(1+\epsilon^2F)(i-F+C_*)\theta_2+i(|\hat{f}|^2+2|\hat{g}|^2)]}{C_*(1+(1+iF-iC_*)\Theta_*)}, \tag{A6}$$

with $\Theta_*=\epsilon^2\theta_*$. The same equation holds for $\hat{g}$ by interchanging $f\leftrightarrow g$ and $F\leftrightarrow G$. Because of the form of the equations for $\hat{f}$ and $\hat{g}$, it is easier to study the equations for $f=|\hat{f}|^2$ and $g=|\hat{g}|^2$ given by

$$\frac{df}{d\rho}=f[C_2C_F+\theta_2\theta_F+a(f+2g)], \tag{A7a}$$

$$\frac{dg}{d\rho}=g[C_2C_G+\theta_2\theta_G-a(g+2f)], \tag{A7b}$$

with

$$a=-\frac{2\Theta_*\sqrt{C_*^2-1}}{1+2\Theta_*+C_*^2\Theta_*^2}, \tag{A8a}$$

$$\theta_F=-(1+\epsilon^2F)a/\Theta_*, \tag{A8b}$$

$$\theta_G=(1+\epsilon^2G)a/\Theta_*, \tag{A8c}$$

$$C_F=\frac{a[1+(1-C_*F+F^2)\Theta_*]}{C_*\Theta_*(C_*-F)}, \tag{A8d}$$

$$C_G=\frac{-a[1+(1-C_*G+G^2)\Theta_*]}{C_*\Theta_*(C_*-G)}. \tag{A8e}$$

A numerical evaluation of all the parameters used here are given in Table II for point P_1 of Fig. 4.

Equations (A7a) and (A7b) admit four steady states [28] (see Fig. 5). The trivial solution

$$f=g=0 \tag{A9}$$

TABLE II. Numerical values of the parameters appearing in Eqs. (A7a)–(A7b). They correspond to the double Hopf point P_1 of Fig. 4 that is found at $\tau \simeq 1941.96$.

Parameter	Symbol	Value
	ϵ	0.177823
Double Hopf critical θ	θ_*	61.410038
Double Hopf critical C	C_*	1.541030
1st Hopf frequency	F	2.713536
2nd Hopf frequency	G	0.368523
$\Theta_* = \epsilon^2 \theta_*$	Θ_*	1.941956
	a	−0.329049
	θ_F	0.183982
	θ_G	−0.171416
	C_F	0.855295
	C_G	0.197198

corresponds to the laser steady state. It exists for every value of C_2 and $\theta_2 = \pm 1$. It is stable only for $C_2 < \min(-\theta_2\theta_F/C_F, -\theta_2\theta_G/C_G)$.

The second solution is

$$f = -(C_2C_F + \theta_2\theta_F)/a, \quad g = 0. \tag{A10}$$

It corresponds to a periodic solution emerging from a supercritical Hopf bifurcation. Because $f = |\hat{f}|^2 \geqslant 0$, this solution exists only for $C_2 \geqslant -\theta_2\theta_F/C_F$. If $\theta_2 = -1$, it is always unstable. If $\theta_2 = +1$, it is stable up to $C_2 = C_{2,F} \equiv -(2\theta_F + \theta_G)/(2C_F + C_G)$ where it is destabilized by a Hopf bifurcation.

The third solution is given by

$$f = 0, \quad g = (C_2C_G + \theta_2\theta_G)/a. \tag{A11}$$

It corresponds to a periodic solution emerging from a subcritical Hopf bifurcation. Because $g = |\hat{g}|^2 \geqslant 0$, this solution exists only for $C_2 \leqslant -\theta_2\theta_G/C_G$. It is always unstable. If $\theta_2 = +1$, a Hopf bifurcation is found at $C_2 = C_{2,G} \equiv -(2\theta_G + \theta_F)/(2C_G + C_F)$.

Finally, the fourth solution is the mixed mode solution given by

$$f = [C_2(C_F + 2C_G) + \theta_2(\theta_F + 2\theta_G)]/3a, \tag{A12a}$$

$$g = -[C_2(C_G + 2C_F) + \theta_2(\theta_G + 2\theta_F)]/3a. \tag{A12b}$$

It corresponds to a two-frequency quasiperiodic regime. Because $f \geqslant 0$ and $g \geqslant 0$, this solution exists only for $\theta_2 = +1$ and $C_{2,F} \leqslant C_2 \leqslant C_{2,G}$. It is stable for $C_2 < C_{2,*} \equiv -(\theta_F + \theta_G)/(C_F + C_G)$. At $C_2 = C_{2,*}$, the solution is destabilized by a Hopf bifurcation that introduces a third frequency in the laser dynamics. The branch that emerges from this bifurcation is thus characterized by three incommensurate frequencies. It is vertical as demonstrated by the existence of the invariant quadrature $fg\{f + g + (C_G\theta_F - C_F\theta_G)/[a(C_F + C_G)]\}$. A higher order analysis is necessary if we wish to determine the direction of bifurcation. Bifurcation diagrams of the pure and mixed mode solutions are shown in Fig. 5.

[1] J.R. Tredicce, F.T. Arecchi, G.L. Lippi, and G.P. Puccioni, J. Opt. Soc. Am. B **2**, 173 (1985).
[2] D. Lenstra, B.H. Verbeck, and A.J. den Boef, IEEE J. Quantum Electron. **QE-21**, 674 (1985).
[3] N.G. Basov, V.N. Morosov, and A.N. Oraevsky, IEEE J. Quantum Electron. **QE-2**, 542-548 (1966).
[4] V.N. Morozov, J. Opt. Soc. Am. B **5**, 909 (1988).
[5] G.L. Oppo and A. Politi, Z. Phys. B: Condens. Matter **59**, 111 (1985); G.-L. Oppo and A. Politi, Phys. Rev. A **40**, 1422 (1989).
[6] T. Erneux, S.M. Baer, and P. Mandel, Phys. Rev. A **35**, 1165 (1987).
[7] T.-C. Yen, J.-W. Chang, J.-M. Lin, and R.-J. Chen, Opt. Commun. **150**, 158 (1998).
[8] K. Otsuka and J.L. Chern, Opt. Lett. **16**, 1759 (1991).
[9] E.V. Grigorieva, S. Kaschenko, N.A. Loiko, and A.M. Samson, Physica D **59**, 297 (1992).
[10] D. Pieroux and T. Erneux, Phys. Rev. A **53**, 2765 (1996).
[11] J.D. Farmer, Physica D **4**, 366 (1982).
[12] C. Risch and C. Voumard, J. Appl. Phys. **48**, 2083 (1977).
[13] G.H.M. van Tartwijk, A.M. Levine, and D. Lenstra, IEEE J. Sel. Top. Quantum Electron. **1**, 466 (1995).
[14] D. Pieroux, T. Erneux, and K. Otsuka, Phys. Rev. A **50**, 1822 (1994).
[15] E.V. Grigorieva, H. Haken, and S.A. Kaschenko, Opt. Commun. **165**, 279 (1999).
[16] R. Lang and K. Kobayashi, IEEE J. Quantum Electron. **QE-16**, 347 (1980).
[17] H. Yasaka, Y. Yoshikuni, and H. Kawaguchi, IEEE J. Quantum Electron. **QE-27**, 193 (1991).
[18] F.T. Arecchi, W. Gadomski, and R. Meucci, Phys. Rev. A **34**, 1617 (1986).
[19] G. Giacomelli, M. Calzavara, and F.T. Arecchi, Opt. Commun. **74**, 97 (1989).
[20] C.-H. Lee, S.-Y. Shin, and S.-Y. Lee, Opt. Lett. **13**, 464 (1988).
[21] F.T. Arecchi, G. Giacomelli, A. Lapucci, and R. Meucci, Phys. Rev. A **43**, 4997 (1991).
[22] N.A. Loiko and A.M. Samson, Opt. Commun. **93**, 66 (1992).
[23] E.V. Grigorieva and S. Kaschenko, Opt. Commun. **102**, 183 (1993).
[24] M.J. Bünner, G. Giacomelli, and A. Politi, J. Opt. B: Quantum Semiclassical Opt. **1**, 171 (1999).
[25] D. Pieroux, Ph.D. thesis, ULB, 1997.
[26] G. Giacomelli and A. Politi, Phys. Rev. Lett. **76**, 2686 (1996); Physica D **117**, 26 (1998).
[27] G. Iooss and W.L. Langford, Ann. N.Y. Acad. Sci. **357**, 489 (1980).
[28] J.M. Guckenheimer and P.J. Holmes, *Nonlinear Oscillations, Dynamical Systems and Bifurcations of Vector Fields* (Springer-Verlag, New York, 1990).
[29] K. Engelborghs, T. Luzyanina, K. in't Hout, and D. Roose,

SIAM J. Sci. Comput. **22**, 1593 (2000); K. Engelborghs, T. Luzyanina, and D. Roose, J. Comput. Appl. Math. **125**, 265 (2000); K. Engelborghs, ''DDE-BIFTOOL: a Matlab package for bifurcation analysis of delay differential equations,'' http://www.cs.kuleuven.ac.be/~koen/delay/ddebiftool.shtml

[30] G.H.M. van Tartwijk and D. Lenstra, Quantum Semiclassic. Opt. **7**, 87 (1995).

[31] D. Lenstra, Opt. Commun. **81**, 209 (1991).

[32] A. Ritter and H. Haug, J. Opt. Soc. Am. B **10**, 130 (1993).

[33] T. Erneux, Proc. SPIE **3944**, 588 (2000).

[34] D. Pieroux, T. Erneux, A. Gavrielides, and V. Kovanis, SIAM J. Appl. Math. **61**, 966 (2000).

[35] E. Hairer, S.P. Norsett, and G. Wanner, *Solving Ordinary Differential Equations*, 2nd rev. ed. (Springer-Verlag, Berlin, 1992), Vol. 1.